Biogeosciences Discuss., 11, 6755–6792, 2014
www.biogeosciences-discuss.net/11/6755/2014/
doi:10.5194/bgd-11-6755-2014

Biogeosciences Discussions
Open Access

Rapid acidification of mode and intermediate waters in the southwest Atlantic Ocean

L. A. Salt[1,*], S. M. A. C. van Heuven[2], M. E. Claus[3], E. M. Jones[4], and H. J. W. de Baar[1,3]

[1]Royal Netherlands Institute for Sea Research, Landsdiep 4, 1797 SZ, Texel, the Netherlands
[2]Centre for Isotope Research, University of Groningen, Nijenborgh 4, 9747 AG, Groningen, the Netherlands
[3]Department of Ocean Ecosystems, University of Groningen, Nijenborgh 7, 9747 AG, Groningen, the Netherlands
[4]Alfred Wegener Institute for Polar and Marine Research, 120161, 27515, Bremerhaven, Germany
[*]now at: CNRS, UMR 7144, Equipe Chimie Marine, Station Biologique de Roscoff, Place Georges Teissier, 29680 Roscoff, France

Received: 20 March 2014 – Accepted: 23 March 2014 – Published: 12 May 2014

Correspondence to: L. A. Salt (lesley.salt@sb-roscoff.fr)

Published by Copernicus Publications on behalf of the European Geosciences Union.

Abstract

Observations along the southwest Atlantic WOCE A17 line made during the Dutch GEOTRACES-NL program (2010–2011) were compared with historical data from 1994 to quantify the changes in the anthropogenic component of the total pool of dissolved inorganic carbon (ΔC_{ant}). Application of the extended Multi Linear Regression (eMLR) method shows that the ΔC_{ant} from 1994 to 2011 has largely remained confined to the upper 1000 dbar. The greatest changes occur in the upper 200 dbar in the Sub-Antarctic Zone (SAZ), where a maximum increase of 37 µmol kg^{-1} is found. South Atlantic Central Water (SACW) experienced the highest rate of increase in C_{ant}, at 0.99 ± 0.14 µmol kg^{-1} yr^{-1}, resulting in a rate of decrease in pH of -0.0016 yr^{-1}. The highest rates of acidification relative to ΔC_{ant}, however, were found in SubAntarctic Mode Water (SAMW) and Antarctic Intermediate Water (AAIW). The low buffering capacity of SAMW and AAIW combined with their relatively high rates of C_{ant} increase of 0.53 ± 0.11 µmol kg^{-1} yr^{-1} and 0.36 ± 0.06 µmol kg^{-1} yr^{-1}, respectively, will lead to rapid acidification in the SAZ and simultaneously reduce the chemical buffering capacity of this significant CO_2 sink.

1 Introduction

The Atlantic Ocean contains the largest store of anthropogenic carbon (C_{ant}) of all the world's oceans, accounting for approximately 38 % of the total C_{ant} inventory (Sabine et al., 2004). Within the Atlantic, the North Atlantic is currently responsible for the majority of the uptake of C_{ant} (Levine et al., 2011), due to the formation of North Atlantic Deep Water (NADW). However, a recent Atlantic basin inventory analysis indicates that in the past decade the South Atlantic has been more effective at sequestering C_{ant} (Wanninkhof et al., 2010) than the North Atlantic. These authors calculated a rate of increase of the North Atlantic inventory of 1.9 Pg C decade^{-1}, whereas the South Atlantic inventory grew at a rate of 3.0 Pg C decade^{-1}. Calculations by Ríos et al. (2012)

BGD
11, 6755–6792, 2014

indicate that the southwestern Atlantic Ocean dominates the South Atlantic sink of C_{ant}, with a storage rate of 0.25 ± 0.035 Pg C decade^{-1}. Quantifying the exact rate of increase in anthropogenic carbon in ocean waters is inherently problematic due to the highly variable nature of DIC within the ocean and the relatively small fraction of total dissolved inorganic carbon (DIC) that the anthropogenic component represents (~ 3 %; Ríos et al., 2010). In the past decade a number of methods for calculating the increase in C_{ant} (ΔC_{ant}) between reoccupation of ocean transects have been developed (TrOCA, φC_T^0, eMLR). Despite the differing approaches and assumptions, there is overall coherence in the determinations of the anthropogenic component of inorganic carbon in the world's oceans (Lee et al., 2003; Peng et al., 2003, 2010; Álvarez et al., 2009; Wanninkhof et al., 2010).

The southwest Atlantic has been occupied several times over the past 20 years and several techniques to determine C_{ant} have been applied to the WOCE '94 A17 transect by Ríos et al. (2010). These methods included ΔC^* (Gruber et al., 1996), Tracer combining Oxygen, inorganic Carbon and total Alkalinity (TrOCA) (Touratier et al., 2007), φC_T^0 (Vázquez-Rodríguez et al., 2009a), and Transit Time Distributions (TTD) (Waugh et al., 2006) and showed general conformity in the distribution of C_{ant}. The presence of the western boundary current in the South Atlantic Ocean means that the C_{ant} signal penetrates deeper and is larger in the western half of the basin compared to the eastern half (Wanninkhof et al., 2010; Ríos et al., 2010; Vázquez-Rodríguez et al., 2009a). Murata et al. (2008) show that the C_{ant} signal in SubAntarctic Mode Water (SAMW) can be ~ 7 µmol kg^{-1} higher west of 15° W compared to the east. The major pathways of C_{ant} into the South Atlantic Ocean interior are by means of the formation of mode and intermediate waters (McNeil et al., 2001; Sabine et al., 2004). The SAMW is formed in the Subantarctic Zone (SAZ), between the Subtropical Front (STF) and subAntarctic Front (SAF), where a calculated anthropogenic CO_2 uptake of 0.07–0.08 Pg C yr^{-1} occurs (Sabine et al., 1999; McNeil et al., 2001). A total CO_2 sink of 1.1 Pg C yr^{-1} has been calculated by McNeil et al. (2007) for the SAZ, making it the largest CO_2 sink in the Southern Ocean and a significant sink for anthropogenic atmospheric CO_2.

BGD
11, 6755–6792, 2014

The increase in DIC that results from the uptake of anthropogenic CO_2 from the atmosphere leads to increasing proton, bicarbonate ion and carbon dioxide concentrations ($[H^+]$, $[HCO_3^-]$,$[CO_2]$) and decreasing carbonate concentrations ($[CO_3^{2-}]$), a process referred to as *ocean acidification*. Sabine et al. (2004) state that approximately 50 % of the total amount of C_{ant} in the world's oceans resides in the upper 400 m. The associated decrease in pH has been calculated as −0.1 pH units in the surface ocean relative to pre-industrial times (Raven et al., 2005; Orr et al., 2005). In the North Atlantic Ocean acidification rates of $-0.0016 \pm 0.0001\,yr^{-1}$ and $-0.0012 \pm 0.002\,yr^{-1}$, for Subarctic Intermediate Water (SAIW) and SubPolar Mode Water (SPMW), respectively, have been reported (Vázquez-Rodríguez et al., 2012). Data from the European Time Series in the Canary Islands (ESTOC) station shows significantly higher rates of pH decrease in surface waters of $0.0017 \pm 0.0004\,yr^{-1}$, for the time period 1995 to 2004 with notable influence from regional climatic forcing (Santana-Casiano et al., 2007). Acidification rates that deviate from the rate that is expected from C_{ant} increases alone have been observed in upper Labrador Sea Water (uLSW), SAIW, and eastern North Atlantic Central Water (eNACW) (Vázquez-Rodríguez et al., 2012). These variations have been attributed to a combination of climatic and biological effects. The greater sensitivity of some water masses to acidification has been well documented by González-Dávila et al. (2011) through application of the buffering factors described by Egleston et al. (2010) and previously Frankignoulle (1994). González-Dávila et al. (2011) highlighted waters originating at high latitudes as particularly sensitive to increases in the concentration of dissolved CO_2 ($[CO_2(aq)]$), in particular Antarctic Intermediate Water (AAIW) and upper Circumpolar Deep Water (*u*CDW) due to low total alkalinity (A_T) to DIC ratios.

A number of the biological consequences of ocean acidification are related to the changes in carbonate, and thus calcium carbonate ($CaCO_3$), ion concentration. Carbonate ions are used by marine calcifying organisms to form both varieties of calcium carbonate: aragonite (e.g. by pteropods) and calcite (e.g. by coccolithophores and foraminifera). Aragonite is the less metastable form of $CaCO_3$ resulting in a satu-

BGD
11, 6755–6792, 2014

ration horizon ($\Omega_{Ar} = 1$) approximately 2 km shallower than that of calcite in the South Atlantic Ocean, below which depth $CaCO_3$ is no longer present in particulate form. A number of experiments have observed shell dissolution in pteropods incubated at elevated partial pressure of CO_2 (pCO_2) (Orr et al., 2005; Lischka et al., 2011) associated with a lowering of the aragonite saturation state. Recently similar results have been observed in situ in the Southern Ocean (Bednaršek et al., 2012), indicating that species are already being affected by C_{ant} accumulation. Organisms that use aragonite are thus much more vulnerable to decreases in $[CO_3^{2-}]$ driven from the surface increase in $[CO_2]$.

This study examines the increase of C_{ant} in the southwest Atlantic Ocean between two occupations of the WOCE A17 line, which took place in 1994 and 2010/11. We calculate the changes in C_{ant} (ΔC_{ant}) in the different water masses and subsequently examine the pH changes driven by the invasion of anthropogenic carbon between WOCE '94 A17 and GEOTRACES-NL (2010/2011). These results are furthermore put into context with regard to the differing buffering capacities of individual water masses.

2 Data and method

2.1 Datasets

The two datasets used in this study are the results from the CO_2 survey data from the WOCE '94 A17 section (public data at: http://cdiac.ornl.gov/oceans/woce_a17c.html) and the Dutch West Atlantic GEOTRACES program, completed in 2011 (GEOTRACES-NL (2010/2011). The respective cruise tracks are shown in Fig. 1. The GEOTRACES-NL (2010/2011) section was carried out in two parts. The shown stations north of the equator were occupied in July 2010 by the Dutch RV Pelagia (expedition 64PE321, from Hamilton, Bermuda to Fortaleza, Brazil), and the Southern Hemisphere was sampled during March 2011 by the British RRS James Cook (JC057, from Punta Arenas, Chile to Las Palmas, Gran Canaria). The WOCE '94 A17 section was similarly

BGD
11, 6755–6792, 2014

carried out in austral autumn and this data has undergone rigorous quality control (Key et al., 2010). The data report is available from "http://cdiac.ornl.gov/oceans/ndp_084/" (Ríos et al., 2005b), where an offset of $-8\,\mu mol\,kg^{-1}$ in the total alkalinity (A_T) data has been reported and corrected for in this study. For a detailed analysis of the WOCE occupation we refer the reader to Ríos et al. (2010).

2.2 GEOTRACES-NL (2010/11) measurements

2.2.1 Dissolved inorganic carbon and total alkalinity

During the GEOTRACES-NL (2010/2011) cruises, for measurements of DIC and A_T, water samples of 600 mL were collected from throughout the water column, from 24 Niskin samplers mounted onto a CTD rosette, following standard operating procedures (Dickson et al., 2007). At least two duplicates samples were collected at each station, from different parts of the profile. Samples were analyzed immediately after collection on a VINDTA 3C (Versatile INstrument for the Determination of Total Alkalinity, Marianda, Kiel) instruments, simultaneously. This system determines DIC by coulometric titration using a coulometer (Johnson et al., 1987) and determines A_T by potentiometric titration with 0.1 M hydrochloric acid (Mintrop et al., 2000). Quality control was performed through regular measurements of certified reference material (CRM, Batch #100) supplied by Andrew Dickson at Scripps Institute of Oceanography (San Diego, California). Based on the measurements performed on the CRM, DIC was measured with a precision of one standard deviation of $1.0\,\mu mol\,kg^{-1}$ and the precision of A_T had one standard deviation of $1.1\,\mu mol\,kg^{-1}$.

2.2.2 Ancillary parameters

Dissolved oxygen samples were collected from a minimum of three depths throughout the water column for CTD sensor calibration. The samples were collected in 120 mL borosilicate glass bottles and treated following the Winkler method (Winkler, 1888) and

BGD
11, 6755–6792, 2014

analyzed spectrophotometrically on a Hitachi U-1100 Spectrophotometer, following Pai et al. (1993). The precision, estimated from 123 replicates, was ±0.98 µmol L^{-1}.

Inorganic nutrients (PO_4, $Si(OH)_4$, NO_3) were analyzed following the methods of Grasshoff et al. (1983). In every run a control and a natural sterilized, Reference Nutrient Sample (RMNS Kanso, Japan) were measured. Precision was estimated to be ±0.01, 0.2, and 0.2 µmol L^{-1} for PO_4, $Si(OH)_4$, and NO_3, respectively. Values of salinity are reported on the practical salinity scale.

2.2.3 pH Calculations

From DIC, A_T and supplementary data (salinity, temperature, pressure, $Si(OH)_4$, PO_4), the pH and pCO_2 were also calculated in-situ for both datasets using CO2_SYS (Lewis and Wallace, 1998) adapted for Matlab (van Heuven, 2011a), applying the acid dissociation constants of Mehrbach et al., (refit by Dickson and Millero, 1987), and the KSO_4 constant of Dickson (1990). The same calculation was carried out for both the WOCE '94 A17 and GEOTRACES-NL (2010/2011) datasets with the resulting pH reported on the total pH scale.

2.3 Deepwater consistency between WOCE and GEOTRACES

In a later section, we employ the eMLR method (Friis et al., 2005) to infer ΔC_{ant} between the two cruises. The eMLR method considers various biogeochemical properties (in this case, salinity, DIC, NO_3, $Si(OH)_4$ and apparent oxygen utilization (AOU = $[O_2]_{sat} - [O_2]_{obs}$)) and is particularly sensitive to large scale ("secular") changes in the distributions of these properties, as well as to analytical biases in their measurement. In order to assess the magnitude and distributions of these changes, we gridded the values of salinity, DIC, NO_3, $Si(OH)_4$ and AOU of each dataset and subtracted the grids from each other. Grid spacing was every 2° of latitude, with 80 layers in the vertical direction, with increased density towards the surface. The differences deeper than 400 dbar (i.e., the deepest extent of the winter mixed layer; Dong et al., 2008) are very

BGD
11, 6755–6792, 2014

modest, having average values (for S, DIC, NO_3, $Si(OH)_4$ and AOU) of 0.004 ± 0.047; $1.5 \pm 12.2\,\mu mol\,kg^{-1}$; $2.15 \pm 6.37\,\mu mol\,kg^{-1}$; $-3.7 \pm 11.5\,\mu mol\,kg^{-1}$; $1.2 \pm 15.0\,\mu mol\,kg^{-1}$, respectively. One would expect greater variability in the upper 400 m, however, the differences remain of a similar order of magnitude with average differences of 0.122 ± 0.404 ; $6 \pm 18\,\mu mol\,kg^{-1}$; $3.51 \pm 8.02\,\mu mol\,kg^{-1}$; $1.4 \pm 3\,\mu mol\,kg^{-1}$; $0.9 \pm 19\,\mu mol\,kg^{-1}$ for S, DIC, NO_3, $Si(OH)_4$ and AOU, respectively.

2.4 eMLR and C_{ant} calculations

There are two general carbon data-based approaches for studying the increasing oceanic C_{ant}. The first approach uses back-calculation techniques (e.g. φC_T, ΔC^*, TrOCA) to obtain an estimate of pre-industrial DIC concentration against which to compare current measurements. Methods from the second approach aim to determine the part of change in DIC between two specific time periods that is attributable to anthropogenic invasion (e.g. multi-linear regression, time series residuals). One example of each approach is employed in this study (eMLR , Friis et al., 2005; and φC_T, Vázquez-Rodríguez et al., 2009a, b). Various comparison and evaluations of these and other methods are available in the literature (Levine et al., 2008; Yool et al., 2010; van Heuven et al., 2011b; Sabine and Tanhua, 2010).

2.4.1 ΔC_{ant} from eMLR

The multi-linear regression approach to estimating anthropogenic CO_2 invasion was introduced by Wallace (1995). It involves using a number of biogeochemical properties, known to be related to DIC, to obtain a model of the observed DIC. As the relationships between DIC and these properties are expected not to change over time, the same statistical relationships can be applied to a second dataset of later date. Differences between the thus "predicted" DIC and the observed DIC are attributed to the invasion of anthropogenic CO_2. In the extended version (eMLR), which is applied here, the DIC from both datasets is fitted to the same selection of properties from both datasets,

BGD
11, 6755–6792, 2014

and the difference between parameter coefficients is assumed to be predictive of the difference in C_{ant} between the two cruises:

$$\Delta C_{ant}^{eMLR} = DIC^{MLR2,t2} - DIC^{MLR1,t1} \quad (1)$$

$$= (a_2 - a_1) + (b_2 - b_1)SiO_{2t2} + (c_2 - c_1)NO_{3t2} + (d_2 - d_1)AOU_{t2} + (e_2 - e_1)S_{t2} + (f_2 - f_1)T_{t2}. \quad (2)$$

Using a stepwise regression the most significant terms for the WOCE A17 '94 dataset were determined as, in order of decreasing importance: S, SiO_2, NO_3, T, and AOU. These properties predict DIC with an R^2 value of 0.99 and a rmse of 6.66 µmol kg^{-1}. For the GEOTRACES-NL (2010/2011) dataset, the order of importance was: S, SiO_2, NO_3, T and AOU, with an R^2 of 0.98 and rmse of 9.87 µmol kg^{-1} (Fig. 2).

The eMLR regressions were applied along isopycnals intervals, as the preferred method of water movement from the surface into the ocean interior is along surfaces of constant density, it thus follows that waters occupying the same density band share a common formation history and can be described by a single equation. Isopycnal bands were chosen based on temperature-salinity plots of the water masses and the amount of data occupying each interval. The coefficients and accompanying statistics from each isopycnal interval are displayed in Table 1. The residuals of each fit are shown in Fig. 2, with the 2011 dataset showing a maximum of 7 µmol kg^{-1}, in the surface layer and an overall average of 2.1 µmol kg^{-1} in the deeper waters (> 2000 dbar). In comparison, the WOCE '94 A17 dataset shows a water column average residual of 3.17 µmol kg^{-1}, which we attribute to less precise measurements in the earlier dataset. Pressure was included in the regression to avoid skewing (over depth) of the residuals of the MLR by the relatively large amount of samples located towards the surface, as mentioned by Hauk et al. (2010).

BGD
11, 6755–6792, 2014

2.4.2 C_{ant} from φC_T^0

The φC_T^0 method is a back-calculation approach that uses stoichiometric ratios from biogeochemical processes to account for the addition of DIC in the water column resulting from organic matter remineralization and calcium carbonate dissolution, since the time of water formation. It is based on the general principle of "preformed DIC" (or C_T^0) of Brewer (1978) and ΔC^* of Gruber et al. (1996), however, the main advantage of this method is that it considers the non-steady state of A_T and pCO_2 in the subsurface reference layer.

2.5 Buffer factors

The Revelle factor was originally described by Revelle and Suess (1957) and quantified the attenuated response of increasing DIC impacted by increasing pCO_2, or vice versa. This work has been built upon by Frankignoulle (1994) and more recently by Egleston et al. (2010), who outlined six expressions that define how $[CO_2]$, $[H^+]$, and Ω_{Ar} or Ω_{Ca}, are impacted by changes in DIC or A_T. The following three equations, taken from Egleston et al. (2010), are the expressions for the three buffer factors relating to DIC and were applied to the GEOTRACES-NL (2010/2011) southwest Atlantic section:

$$\gamma\mathrm{DIC} = (\partial \ln[CO_2]/\partial \mathrm{DIC})^{-1} = \mathrm{DIC} - \mathrm{Alk_C}^2/S, \quad (3)$$

$$\beta\mathrm{DIC} = (\partial \ln[H^+]/\partial \mathrm{DIC})^{-1} = \mathrm{DIC} \times S - \mathrm{Alk_C}^2/\mathrm{Alk_C}, \quad (4)$$

$$\omega\mathrm{DIC} = (\partial \ln \Omega/\partial \mathrm{DIC})^{-1} = \mathrm{DIC} - \{\mathrm{Alk_C} \times P/[HCO_3^-]\}, \quad (5)$$

$$\text{where } \mathrm{DIC} = [CO_2] + [HCO_3^-] + [CO_3^{2-}], \quad (6)$$

$$\mathrm{Alk_C} = [HCO_3^-] + 2[CO_3^{2-}], \quad (7)$$

$$P = 2[CO_2] + [HCO_3^-], \quad (8)$$

$$S = [HCO_3^-] + 4[CO_3^{2-}] + [H^+] + [OH^-] + \{[H^+][B(OH)_4^-]/\mathrm{Khb} + [H^+]\} \quad (9)$$

BGD
11, 6755–6792, 2014

and Ω refers to the saturation state of sea water with respect to aragonite or calcite. These equations quantify the resistance to change of $[CO^2]$ (γDIC), $[H^+]$ (βDIC) and Ω (ωDIC) in a water mass to changes in DIC. The concentrations used for the calculations were obtained from CO2SYS (Lewis and Wallace, 1998, adapted for Matlab by van Heuven, 2011a) using the same input conditions as previously mentioned (Sect. 2.2.3).

3 Hydrography of the South Atlantic Ocean

The distributions of potential temperature, salinity, AOU, silicate, A_T, and DIC of the GEOTRACES-NL (2010/2011) section are shown in Fig. 3. The large water masses have been described elsewhere (Mémery et al., 2000; Ríos et al., 2010; Wanninkhof et al., 2010), thus here the treatment is relatively brief. Located deeper than 4500 dbar throughout the section is Antarctic Bottom Water (AABW), characteristic in its high DIC and AOU. Values for DIC in this water mass range from 2243 to 2267 µmol kg^{-1}, and AOU values occupy a narrow band between 111 to 128 µmol kg^{-1}. The DIC maximum (2267 µmol kg^{-1}) and potential temperature minimum (−0.16 °C) are both found in this water mass, which also shows the deep water A_T maximum (2369 µmol kg^{-1}), occurring below the upper 1000 m. These characteristics are all representative of the old age of the water mass and are caused by the large amount of organic matter remineralization which has taken place within it. The AABW can, most easily, be distinguished from the overlying *lower* Circumpolar Deep Water (*l*CDW), by the high silicate concentrations, which reach values greater than 120 µmol kg^{-1} in AABW. Silicate concentrations in the deep waters (> 4000 dbar) demonstrate a strong covariance with A_T (R^2 = 0.95), which has been previously noted (Broecker and Peng, 1982; Ríos et al., 1995; Pérez et al., 2002) and stems from the simultaneous dissolution of opaline and calcium carbonate shells from the hard tissue of organisms (Pérez et al., 2002).

The *l*CDW has a core at approximately 3500 dbar at 50° S, above which it merges into *upper* Circumpolar Deep Water (*u*CDW), with its respective core identified by an oxygen minimum at approximately 1500 m (Mémery et al., 2000). Both branches

BGD
11, 6755–6792, 2014

of CDW display properties similar to that of AABW, as they represent a mixture of AABW and Weddell Sea Deep Water (Wong et al., 1999; Orsi et al., 1999). The *u*CDW and /CDW share isopycnals with *upper* North Atlantic Deep Water (*u*NADW) and *lower* North Atlantic Deep Water (/NADW), respectively, in the northern half of the section. The *u*CDW and *u*NADW, occupy the density band between $\sigma_\theta > 27.4$ and $\sigma_3 < 41.47$, with the front between the two water masses found at approximately 26° N (Mémery et al., 2000). The NADW has been more recently ventilated than CDW and is thus distinguished by lower AOU values of $\sim 60\,\mu mol\,kg^{-1}$ and DIC values lower than $2200\,\mu mol\,kg^{-1}$. The deeper /NADW can be separated from *u*NADW through higher silicate values, which rise to $40\,\mu mol\,kg^{-1}$, whereas *u*NADW has maximum silicate concentrations of $20\,\mu mol\,kg^{-1}$ (Fig. 3d). The A_T values are also lower ($\sim 20\,\mu mol\,kg^{-1}$) in *u*NADW compared to /NADW.

The Antarctic Intermediate Water (AAIW) enters the section at 200 dbar just south of 48° S, identifiable as a tongue of water with very low salinity and A_T (34.05 and $2275\,\mu mol\,kg^{-1}$, respectively). The AAIW lies above *u*CDW and below SubAntarctic Mode Water (SAMW) (Peterson and Whitworth, 1989). This water mass is carried northward at intermediate depths between $\sigma_\theta > 27.1$ and $\sigma_\theta < 27.4$ (Ríos et al., 2012) from south of the SAF. In the southwestern Atlantic Ocean AAIW extends further north than in other oceans, due to the western boundary current along the coast of South America (Talley, 1996). The AAIW is a relatively young water mass and has AOU values comparable to NADW (~ 50–$100\,\mu mol\,kg^{-1}$), however, it can be distinguished from *u*NADW, in its northward reaches, by its elevated silicate concentrations. Situated above the AAIW, the SAMW is often considered a component of the AAIW (McCartney, 1977). This water mass can be easily identified by the tracer $Si^* = [Si(OH)_4] - [NO_3^-]$ which has values from -10 to $-15\,\mu mol\,kg^{-1}$ in regions of SAMW formation (Sarmiento et al., 2004). The SAMW formation region is located just south of 47° S in the Subantarctic Zone (SAZ), north of the SAF (McCartney, 1977) where deep winter mixing forms this high-oxygen water mass.

BGD
11, 6755–6792, 2014

We locate the Subtropical Front (STF) at ~ 41° S, where there is a steep gradient in salinity in the surface 200 dbar. North of the STF, in the surface, and extending northward to a density of $\sigma_\theta < 26.5\,\mathrm{kg\,m^{-3}}$, is South Atlantic Central Water (SACW; Ríos et al., 2012), heavily depleted in silicate, and with elevated salinity and A_T. Against this background, the two Amazon plumes are very distinct at 5° N and 15° N with salinity and A_T values as low as 34.11 and 2265 µmol kg^{-1}, and 32.3 and 2157 µmol kg^{-1}, respectively. The maximum values of both salinity and A_T correspond with South Atlantic Central Water (SACW) in the subtropics (17° S), reaching absolute maxima of 37.5 and 2456 µmol kg^{-1}, respectively, at 50 dbar depth. The subtropical part of the SACW that features high salinity and A_T is often referred to as the Salinity Maximum Water (SMW). In this study we make no distinction between SMW and SACW.

4 Results

4.1 ΔC_{ant} from eMLR

The increase in C_{ant} (ΔC_{ant}) from 1994 to 2011, obtained from an eMLR analysis, is shown in Fig. 4a. The general pattern is that from 1994 to 2011 the most evident increase in C_{ant} occurred in the upper 1000 dbar, particularly in the southern half of the section. The largest increases (up to 36 µmol kg^{-1}) were found in the surface waters of the SAZ, just south of 45° S. Within the surface waters (< 100 dbar) of the section the ΔC_{ant} gradually decreases northwards in a linear relationship with latitude ($R^2 = -0.74$) to a concentration of 0 µmol kg^{-1} just north of the equator (~ 5° N). This follows the pattern expected from surface water temperature, which plays a large role in determining the surface ocean pCO_2 and contributes to the equatorial region acting as a source of CO_2 to the atmosphere during austral summer (Takahashi et al., 2009). The steepest vertical gradient of ΔC_{ant} is found at ~ 47° S just north of the SAF, where over a depth range of 0–600 dbar the ΔC_{ant} decreases from 36 to 0 µmol kg^{-1}.

BGD
11, 6755–6792, 2014

South of 15° S the deepest penetration of positive ΔC_{ant} values is found at 1200 dbar in the STZ, between 25° S and 40° S. The ΔC_{ant} zero-contour shoals southward of 35° S to ~ 600 dbar at 50° S, coinciding with the lower limits of AAIW, as has been noted in other ocean basins (Sabine et al., 2004). In the northern half of the section, the deepest limit of ΔC_{ant} penetration in AAIW reaches a depth of ~ 700 dbar at 15° S and north of the equator the AAIW signal becomes distorted as it mixes with NADW. The NADW shows near-zero concentrations of ΔC_{ant} throughout its extent, with the exception of the *u*NADW in the equatorial region, which show ΔC_{ant} values up to 5 µmol kg^{-1}. In /NADW and the other deep and bottom waters (AABW, /CDW), ΔC_{ant} shows no change or a tendency to negative values.

To estimate the rate of increase of C_{ant} in each water mass we identified their respective cores using the water mass descriptions given in Mémery et al. (2000) and Ríos et al. (2012) and averaged their values of ΔC_{ant}. Assuming a constant yearly increase, we then divided this total increase by 17 to obtain the rate of yearly increase of C_{ant} over the period 1994 to 2011. The calculated values are shown in Table 2 with those of Ríos et al. (2012) for comparison. The highest rates of increase were found in SACW and SAMW with C_{ant} increase rates of 0.99 ± 0.14 µmol kg^{-1} yr^{-1} and 0.53 ± 0.11 µmol kg^{-1} yr^{-1}, respectively. The latter value shows good consistency with that calculated by Ríos et al. (2012; 0.53 ± 0.02 µmol kg^{-1} yr^{-1}). However, there is a notable difference of 0.09 µmol kg^{-1} yr^{-1} between the increase for SACW calculated here and that of 0.90 ± 0.04 µmol kg^{-1} yr^{-1} (Ríos et al., 2012). As this is a surface water mass, and our study utilized data collected 6 years after that used for comparison in Ríos et al. (2012), we corrected the ΔC_{ant} accordingly. Assuming equilibration between the atmosphere and ocean we corrected our ΔC_{ant} value for the additional DIC increase caused solely by atmospheric increases over the last 6 years. The resulting calculated $C_{ant}^{1994–2005}$ increase rate was 0.92 ± 0.14 µmol kg^{-1} yr^{-1}, making our result consistent with the previous estimate. As such, we attribute the difference in calculated ΔC_{ant} increase rates in SACW to the increase in DIC driven by higher atmospheric pCO_2 concentrations in 2010/11. Despite the similarities in formation history between SAMW

BGD
11, 6755–6792, 2014

and AAIW, the latter shows a much lower increase rate of $0.37 \pm 0.06\,\mu mol\,kg^{-1}\,yr^{-1}$. Increase rates of $0.33 \pm 0.07\,\mu mol\,kg^{-1}\,yr^{-1}$ and $0.20 \pm 0.03\,\mu mol\,kg^{-1}\,yr^{-1}$ were calculated for *u*CDW and *u*NADW, respectively. The /NADW, /CDW and AABW all show no significant increases.

4.2 Changes to pH and buffering capacity

Assuming no changes of A_T between the WOCE '94 A17 and GEOTRACES-NL (2010/2011) occupations, we use the calculated ΔC_{ant} and the measured A_T during GEOTRACES-NL (2010/2011) to calculate the anthropogenic driven change in pH from 1994 to 2011 ($\Delta pH^{1994–2011}$). From the application of the φC_T^0 method of anthropogenic carbon determination (Vázquez-Rodríguez et al., 2009a, b; Sect. 2.3.2) we obtain the C_{ant} signal since pre-industrial times, which allows the calculation of the decline in pH, which has occurred since pre-industrial times (ΔpH) (Fig. 4b). The average surface (< 250 dbar) ΔpH, across the section, from pre-industrial times to 1994, calculated using the φC_T^0 method, was −0.08, which is just under the predicted, general surface ocean decrease of 0.1 (Orr et al., 2005). The ocean interior experienced relatively small ΔpH, however, the change was accompanied by a significant shoaling of the aragonite saturation horizon, most notably in the southern half of the section (Fig. 4b). South of the SAF, at ∼ 49° S, the aragonite saturation horizon rose by ∼ 250 m, whereas further north, at 25° S, it has risen just 200 m. The change was almost imperceptible north of the Equator. From 1994 to 2011 the surface pH shows an averaged, further decline of 0.03, making the total surface ΔpH −0.11 since pre-industrial times. Thus, of the total decrease in pH since pre-industrial times to the present day, 27 % occurred within the past 17 years. However, we can detect no notable change to the aragonite saturation state. Historically, the uptake of C_{ant} by the surface ocean was relatively gradual, which allowed it to be well distributed throughout the water column. In contrast, the effects of the more recent, steeply increasing, anthropogenic acidification have not yet significantly penetrated into the deeper ocean.

BGD
11, 6755–6792, 2014

The distribution of $\Delta pH^{1994–2011}$ across the section broadly follows the C_{ant} increases (compare Fig. 4a and b), as expected under the assumption of constant A_T. If we further assume a constant decrease over the 17 years, the yearly acidification rates were calculated from $\Delta pH^{1994–2011}$ and identified for each water mass core, as done for the yearly C_{ant} increases (Table 2). The highest rates of acidification were found in the surface waters, where we also observe the greatest rates of C_{ant} increase, with SACW showing a rate of pH decrease of $-0.0016\,yr^{-1}$. The latter value is in line with that calculated for the same water mass on the eastern side of the North Atlantic Ocean at the ESTOC site ($-0.0017\,yr^{-1}$) for the period 1995 to 2004 (Santana-Casiano et al., 2007; González-Dávila et al., 2011). The SAMW demonstrates the next greatest rate of decline with $-0.0014\,yr^{-1}$, followed by AAIW and *u*CDW both showing acidification rates of $-0.001\,yr^{-1}$, which are comparable with values from other recently ventilated water masses in the North Atlantic: acidification rates of $-0.0019\,yr^{-1}$ and $-0.0012\,yr^{-1}$ have been reported for SubArctic Intermediate Water and SubPolar Mode Water, respectively (Vázquez-Rodríguez et al., 2012). The lowest non-zero acidification rate of $-0.0005\,yr^{-1}$ is found in *u*NADW.

5 Discussion

The distribution of ΔC_{ant} and the increase rates of C_{ant} calculated here show good consistency with previous studies (Ríos et al., 2010; Wanninkhof et al., 2010; Ríos et al., 2012). In contrast to our calculated ΔC_{ant}, a number of studies have found increasing concentrations of C_{ant} in AABW (Murata et al., 2008; Vázquez-Rodríguez et al., 2009a; Brown et al., 2010). However, it has been noted previously that it is absent in eMLR analyses (Wanninkhof et al., 2010). The distributions of C_{ant} in AABW presented in Vázquez-Rodríguez et al. (2009a) also indicate that C_{ant} concentrations have not yet spread further north than 50° S, potentially explaining its absence in our analysis. Analysis of changes in the surface waters are usually overlooked due to the larger residuals

BGD
11, 6755–6792, 2014

associated with the presence of biological activity and seasonal variability (Friis et al., 2005), however, here we give these results validation.

The SAZ is typically under-saturated with respect to CO_2 (Metzl et al., 1999) due to a combination of low temperatures and biological activity (McNeil et al., 2007). Calculation of pCO_2 using DIC and A_T shows that during both the WOCE '94 A17 and GEOTRACES-NL (2010/11) cruises the surface waters in the SAZ were under-saturated with respect to atmospheric pCO_2, at 311.5 µatm and 355.2 µatm, respectively (atmospheric pCO_2 was 359 µatm in 1994 and 392 µatm in 2011, ftp://aftp.cmdl.noaa.gov/products/trends/co2/co2_annmean_mlo.txt). The two years thus show relative consistency in ΔpCO_2 ($pCO_{2\,\mathrm{ocean}} - pCO_{2\,\mathrm{atm}}$.), with an average under-saturation of −47.5 µatm in 1994 and −38.8 µatm in 2011. Using average salinity, A_T, temperature and pressure in this region, this computes as a DIC difference of 4.4 µmol kg^{-1} between the two years. Furthermore, principally the variability in both temperature and biology should be accounted for in the eMLR because of the use of temperature and biology-representative variables used (i.e. temperature, NO_3 and $Si(OH)_4$). However, the conceivably variable carbon export between the two time periods (due to variably dominant phytoplankton groups) may have lead to variation in the chemical stoichiometry, which could not be accounted for.

To corroborate our observations of surface ΔC_{ant} obtained using eMLR by another approach, we follow Lee et al. (1997) to derive a linear relationship between temperature and salinity normalized-DIC (NDIC = DIC$\cdot(35/S)$) for surface waters (< 100 dbar) with a temperature greater than, or equal to, 19 °C ($T \geq 19$) and lower than 19 °C ($T < 19$). We derive such relationships for both WOCE '94 A17 and GEOTRACES-NL (2010/2011) data, with the resulting equations given below with those of Lee et al. (1997):

Lee et al. (1997): $T \geq 19\,^{\circ}\mathrm{C}:\ \mathrm{NDIC} = 2136.3 - 6.97T$ (10)

$T < 19\,^{\circ}\mathrm{C}:\ \mathrm{NDIC} = 2163.2 - 9.15T$ (11)

WOCE (1994): $T \geq 19\,^{\circ}\mathrm{C}:\ \mathrm{NDIC} = 2141 - 6.99T \quad (R^2 = 0.86)$ (12)

BGD
11, 6755–6792, 2014

$$T < 19\,^{\circ}\mathrm{C}: \ \mathrm{NDIC} = 2209 - 10.69T \quad (R^2 = 0.96) \tag{13}$$

GEOTRACES (2011):

$$T \geq 19\,^{\circ}\mathrm{C}: \ \mathrm{NDIC} = 2160 - 7.02T \quad (R^2 = 0.85) \tag{14}$$

$$T < 19\,^{\circ}\mathrm{C}: \ \mathrm{NDIC} = 2246 - 11.09T \quad (R^2 = 0.99) \tag{15}$$

For $T \geq 19\,^{\circ}\mathrm{C}$ the gradient between temperature and NDIC is almost identical for all three datasets, varying from 6.90 to 7.02, which would result in a maximum NDIC difference of 2.6 µmol kg^{-1} at 29.3 °C (the maximum temperature recorded of both datasets). These temperatures cover the tropics to the mid-latitudes, reaching 40° S. The resulting equations, from the WOCE '94 A17 and GEOTRACES-NL (2010/2011) datasets, show an increasing intercept of NDIC of 19 (2160–2141) µmol kg^{-1} from 1994 to 2011, which is consistent with the increase anticipated solely by increasing atmospheric pCO_2 (+20 µmol kg^{-1}). The increase of intercept also falls within the calculated ΔC_{ant} values using eMLR, between latitudes 0° to 40° S (14 to 27 µmol kg^{-1}). North of the equator inconsistencies emerge between the estimated ΔC_{ant} values from the derived equation and from the eMLR analysis. In this region the pCO_2 of the ocean often exceeds that of the atmosphere (Takahashi et al., 2009), thus changes in temperature or other physical processes may exert controls undetectable by our analysis.

The colder temperature range (< 19 °C), encompassing the higher latitudes (> 46° S), shows a slight steepening of the slope over the years in addition to an increased intercept. The observed increase in the intercept of 37 (2246–2209) µmol kg^{-1} corresponds with the highest value of ΔDIC calculated using eMLR (37 µmol kg^{-1} at 49° S) at a temperature of 11.2 °C. The variation in the slope (11.09 – 10.69 = 0.4) leads to a maximum difference of ±7.6 µmol kg^{-1} DIC at 18.9 °C between the calculated NDIC values from 1994 to 2011. This comparison increases our confidence in our ΔC_{ant} values calculated in the surface waters, however, we note that in the high latitude regions there is the potential for greater errors.

The continuing uptake of atmospheric CO_2 gradually depletes the naturally available carbonate ion in the surface ocean thereby decreasing the capacity to "buffer" further CO_2 uptake and leading to the gradual acidification of the seawater. The extent to which

BGD
11, 6755–6792, 2014

the pH is affected by the increase of DIC is dependent upon several properties, including temperature, pressure, and A_T, which together determine its *buffering capacity*. As DIC increases, assuming no other changes take place, the buffering capacity of the water is reduced as $[CO_3^{2-}]$ decreases and $[CO_2]$ increases. The A_T is not altered by the flux of atmospheric CO_2 into the ocean, however, it is affected by biological processes, notably the dissolution and formation of calcium carbonate, with dissolution dominating in deep waters and formation playing a more important role in the surface. Table 2 quantifies the extent to which the calculated ΔC_{ant} have impacted pH in the water masses of the southwest Atlantic Ocean. Examination of this table clearly shows that the rate of acidification per $\mu mol\,kg^{-1}$ of DIC is not equal between water masses. The SAMW, a relatively fresh, low alkalinity water mass, has an acidification rate of $-0.0014\,yr^{-1}$, which is 88 % of that of SACW, a warmer, more saline water mass. However, the C_{ant} increase rate of SAMW is only 54 % that of SACW. The AAIW shows the same rate of acidification as *u*CDW, however, the increase of C_{ant} in *u*CDW is 10 % lower than that of AAIW. These differences can be attributed to the varying buffering capacities of the water masses.

The distributions of the sensitivities of $[H^+]$ (βDIC), $[CO_2]$ (γDIC) and Ω_{CaCO_3} (ωDIC) to changes in DIC for the southwest Atlantic are shown in Fig. 5. The greatest sensitivities to increasing DIC (denoted by low values in Fig. 5a and b, and high values in c) were generally found in the deep waters. That is to say that for a given increase in DIC these waters will show large resultant changes in $[H^+]$, $[CO_2]$ and $[CO_3^{2-}]$, or aragonite and calcite saturation (Ω_{Ar}, Ω_{Ca}). Both *u*CDW and /CDW show very similar behavior – as expected from their similar formation history – however, interestingly, there is a notable difference between the buffering capacities of the two limbs of NADW. The difference is most noticeable in ωDIC, likely caused by the slightly higher A_T/DIC ratio in /NADW. A lower βDIC in *u*NADW denotes a greater sensitivity to acidification in response to increasing DIC concentrations. More rapid acidification in *u*NADW, compared to /NADW, has been observed by Vázquez-Rodríguez et al. (2012) and attributed to mixing with Labrador Sea Water (LSW), which exhibits a strong decreasing

BGD
11, 6755–6792, 2014

pH trend with time. The lower pH of LSW and its contribution to *u*NADW could account for the reduced buffering capacity calculated in this water mass in the southwest Atlantic Ocean.

The highest βDIC values are found in SACW, and SAMW which both have relatively low concentrations of DIC compared to the other water masses but higher concentrations of A_T. The three water masses with the greatest response in pH relative to ΔC_{ant} were AAIW, *u*CDW and /CDW, with βDIC values of 0.148 mmol kg^{-1}, 0.141 mmol kg^{-1}, and 0.143 mmol kg^{-1}, respectively. These water masses show the highest DIC/A_T ratios along the section as they all originate in the Southern Ocean (SO) where upwelling brings deep waters rich in [CO_2(aq)] and low in [CO_3^{2-}] to the surface. In addition, these waters have slightly lower salinities and thus lower borate concentrations, which further diminish their buffering capacity. For the same DIC value the buffering capacity of AAIW is substantially lower than that of *u*CDW stemming from the low A_T of AAIW, which is also reflected in the low ωDIC values. With the current calculated rate of increase of C_{ant}, aragonite will become under-saturated in AAIW around the year 2100, when DIC concentrations reach 2208 µmol kg^{-1}. This could happen even sooner, as wintertime, storm-driven upwelling entrainment of deep waters into the surface in the SO is predicted to cause seasonal aragonite under-saturation in the region as soon as 2030, when atmospheric CO_2 levels reach ~ 450 ppm (McNeil and Matear, 2008).

To quantify the differences between water masses in the context of increasing DIC, we calculate the respective changes in [H^+], [CO_3^{2-}] and pH in response to a 10 µmol kg^{-1} increase in DIC in SACW and *u*CDW. In SACW such an increase would lead to a 3.87 % increase in [H^+] and a 2.51 % decrease in [CO_3^{2-}] with a pH decline of −0.0165. In contrast, the same increase in *u*CDW leads to a +7.3 % increase in [H^+], −6.26 % decrease in [CO_3^{2-}] with pH decreasing by 0.0306 units. This makes *u*CDW twice as susceptible to pH changes from increasing DIC than SACW and three times more susceptible to [CO_3^{2-}] decreases and thus under-saturation of aragonite and calcite.

BGD
11, 6755–6792, 2014

Furthermore, the buffering capacity of each water mass will be reduced by increasing the DIC concentrations. To investigate how the buffering capacities of the different water masses in this section have changed over time, and will continue to do so, the DIC buffer factors of each water mass were calculated and plotted against DIC concentration (Fig. 6). Due to the large relative error of the calculated ΔC_{ant} increases in the deeper waters, these were not included. The high rate of uptake of C_{ant} by SACW means that this water mass has seen the largest decrease in buffering capacity since pre-industrial times. The βDIC value has decreased from 0.281 to 0.247 mmol kg^{-1} and Ω_{Ar} has decreased from 4.1 to 3.3. In contrast, *u*CDW has shown relatively little change due to the low values of C_{ant}. However, extrapolating our calculated C_{ant} rates of increase we predict a 33 µmol kg^{-1} increase in this water mass over the next century, which will result in a significant reduction in buffering and a pH decrease of −0.102. The buffering capacities of SAMW and AAIW follow a similar pattern to each other, however, SAMW contains a greater proportion of subtropical water than AAIW, thus it maintains a slightly higher buffering capacity than AAIW. Both AAIW and *u*CDW will see a similar increase in C_{ant} over the next century (37 and 33 µmol kg^{-1}, respectively), however, the decline in Ω_{Ar} will be 1.6 times greater in AAIW, leading to under-saturation. The SAMW will see approximately 54 % of the increase in C_{ant} that SACW will experience, however will undergo 84 % of the associated pH decline. These changes highlight the vulnerability of SAMW and AAIW to increasing C_{ant}, as noted by Gonzalez-Davila et al. (2011).

The observed pattern of ΔC_{ant} in the southwest Atlantic clearly identifies the SAZ as the most effective entry point of C_{ant} into the ocean. In addition, the buffering factors of Egleston et al. (2010) explicitly show that by the end of this century the two dominant water masses in this area (SAMW and AAIW) will be the most sensitive to further C_{ant} increases. Whilst it is clear that this will accelerate the rate of acidification in these water masses, it is unclear how it will affect the CO_2 uptake in the SAZ. Assuming no changes to primary production, the increased sensitivity of SAMW to DIC changes will lead to much greater seasonal variability in the carbonate system of this water mass between the productive and non-productive period. The biological uptake of DIC in the

BGD
11, 6755–6792, 2014

SAZ in austral spring and summer would lead to a more dramatic decrease in surface water pCO_2, allowing a greater air–sea pCO_2 flux. Conversely, the acidification and decline in Ω_{Ar} may be detrimental to calcifying organisms in the area, as observed in the Southern Ocean (Bednarsek et al., 2012), thus limiting export via the biological pump. Additionally, SAMW plays a vital role in the ventilation and supply of nutrients to the thermocline (Karstensen and Quadfasel, 2002; Sarmiento et al., 2004) with models suggesting that this source of nutrients sustains almost three-quarters of primary production in the low latitudes (Sarmiento et al., 2004). As such, reductions to production and export in these regions may have significant consequences for other areas of the ocean as well.

The water masses SAMW and AAIW both risk further reduction in their buffering capacities by long-term variability to their physical properties. On decadal time scales a freshening of AAIW has been observed in the Pacific and Indian sectors of the Southern Ocean (Wong et al., 1999). Decadal variability has also been noted in temperature, salinity and biogeochemical parameters of SAMW (Bindoff et al., 2007; Alvarez et al., 2011), which could further diminish or enhance the buffering capacity of this water mass and thus the C_{ant} driven acidification. Variations on decadal time scales have been related to the Southern Annular Mode (Álvarez et al., 2011), the dominant climate forcing over the region. Similarly in the North Atlantic, the North Atlantic Oscillation exerts a degree of control over the carbonate system variables and C_{ant} uptake (Santana-Casiano et al., 2007; Pérez et al., 2010). Such external controls will cause irregular C_{ant} uptake over time, as has been observed by Brown et al. (2010), making it difficult to accurately predict future C_{ant} uptake.

6 Conclusion

The continuing uptake of C_{ant} in the southwest Atlantic has been assessed through application of eMLR to two datasets collected in 1994 and 2011. The distribution of ΔC_{ant} is comparable with previous studies of C_{ant} accumulation in the region

BGD
11, 6755–6792, 2014

(Ríos et al., 2010). The largest increases are found in the SAZ, just north of the SAF; a previously identified substantial CO_2 sink (Metzl et al., 1999). The SACW ($0.99 \pm 0.14\,\mu mol\,kg^{-1}\,yr^{-1}$), SAMW ($0.53 \pm 0.11\,\mu mol\,kg^{-1}\,yr^{-1}$) and AAIW ($0.36 \pm 0.06\,\mu mol\,kg^{-1}\,yr^{-1}$) are responsible for the greatest C_{ant} uptake, consistent with earlier studies showing them to be an effective pathway of C_{ant} into the ocean interior (Álvarez et al., 2009). The lower extent of AAIW demarks the greatest depth of penetration of C_{ant} into the ocean in the past 17 years indicating that future uptake will similarly be largely concentrated within the surface 1000 m.

The increase in C_{ant} in the southwest Atlantic has led to acidification of water masses. The calculated C_{ant}-driven acidification is greatest in SACW, where a current rate of pH decline of $0.0016\,yr^{-1}$ is found. However, the acidification response per $\mu mol\,kg^{-1}$ increase in DIC is greatest in the intermediate and mode waters. We identify SAMW as the water mass with the greatest risk of rapid acidification, due to a combination of its high C_{ant} uptake and its limited buffering capacity. AAIW, on the other hand, is more at risk of aragonite under-saturation due its low A_T values and resultant high ωDIC values. Continued increase of C_{ant} at the current rate calculated will lead to aragonite under-saturation in the core of AAIW by 2104.

Acknowledgements. We thank the captains and crews of the Research Vessels Pelagia and the Royal Research Ship James Cook.

References

Álvarez, M., Lo Monaco, C., Tanhua, T., Yool, A., Oschlies, A., Bullister, J. L., Goyet, C., Metzl, N., Touratier, F., McDonagh, E., and Bryden, H. L.: Estimating the storage of anthropogenic carbon in the subtropical Indian Ocean: a comparison of five different approaches, Biogeosciences, 6, 681–703, doi:10.5194/bg-6-681-2009, 2009.

Álvarez, M., Tanhua, T., Brix, H., Lo Monaco, C., Metzl, N., McDonagh, E. L., and Bryden, H. L.: Decadal biogeochemical changes in the subtropical Indian Ocean associated with Subantarctic Mode Water, J. Geophys. Res., 116, C09016, doi:10.1029/2010JC006475, 2011.

BGD
11, 6755–6792, 2014

Bednarsek, N., Tarling, G. A., Bakker, D. C. E., Fielding, S., Jones, E. M., Venables, H. J., Ward, P., Kuzirian, A., Lézé, B., Feely, R. A., and Murphy, E. J.: Extensive dissolution of live pteropods in the Southern Ocean, Nat. Geosci., 5, 881–885, doi:10.1038/NGEO1635, 2012.

Bindoff, N. L., Willebrand, J., Artale, V., A, Cazenave, Gregory, J., Gulev, S., Hanawa, K., Le Quéré, C., Levitus, S., Nojiri, Y., Shum, C. K., Talley, L. D., and Unnikrishnan, A.: Observations: oceanic climate change and sea level, in: Climate Change 2007: The Physical Science Basis, Contribution of Working Group I to the Fourth Assessment Report of the Intergovernmental Panel on Climate Change, edited by: Solomon, S., Qin, D., Manning, M., Chen, Z., Marquis, M., Averyt, K. B., Tignor, M., and Miller, H. L., Cambridge University Press, Cambridge, UK and New York, NY, USA, 2007.

Brewer, P. G.: Direct observation of the oceanic CO_2 increase, Geophys. Res. Lett., 5, 997–1000, 1978.

Broecker, W. S. and Peng, T.-H.: Tracers in the Sea, Columbia University, Eldigio Press, New York, 690 pp., 1982.

Brown, P. J., Bakker, D. C. E., Schuster, U., and Watson, A. J.: Anthropogenic carbon accumulation in the subtropical North Atlantic, J. Geophys. Res., 115, C04016, doi:10.1029/2008JC005043, 2010.

Dickson, A. G.: Standard potential of the reaction: $AgCl(s) + 1/2H_2(g) = Ag(s) + HCl(aq)$, and the standard acidity constant of the ion HSO_4^- in synthetic seawater from 273.15 to 318.15,K, J. Chem. Thermodyn., 22, 113–127, 1990.

Dickson, A. G. and Millero, F. J.: A comparison of the equilibrium constants for the dissociation of carbonic acid in seawater media, Deep-Sea Res., 34, 1733–1743, 1987.

Dickson, A. G., Sabine, C. L., and Christian, J. R. (Eds.): Guide to Best Practices for Ocean CO_2 Measurements, PICES Special Publications 3, 191 pp., 2007.

Dong, S., Sprintall, J., Gille, S. T., and Talley, L.: Southern ocean mixed-layer depth from Argo float profiles, J. Geophys. Res., 113, C06013, doi:10.1029/2006JC004051, 2008.

Egleston, E. S., Sabine, C. L., and Morel, M.: Revelle revisited: buffer factors that quantify the reponse of ocean chemistry to changes in DIC and alkalinity, Global Biogeochem. Cy., 24, GB1002, doi:10.1029/2008GB003407, 2010.

Frankignoulle, M.: A complete set of buffer factors for acid/base CO_2 system in seawater, J. Marine Syst., 5, 111–118, doi:10.1016/0924-7963(94)90026-4, 1994.

BGD
11, 6755–6792, 2014

Friis, K., Körtzinger, A., Patsch, J., and Wallace, D. W. R.: On the temporal increase of anthropogenic CO_2 in the subpolar North Atlantic, Deep-Sea Res. Pt. I, 52, 681–698, doi:10.1016/j.dsr.2004.11.017, 2005.

González-Dávila, M., Santana-Casiano, J. M., Fine, R. A., Happell, J., Delille, B., and Speich, S.: Carbonate system in the water masses of the Southeast Atlantic sector of the Southern Ocean during February and March 2008, Biogeosciences, 8, 1401–1413, doi:10.5194/bg-8-1401-2011, 2011.

Grasshof, K., Ehrhardt, M., and Kremling, K.: Methods of Seawater Analysis, Verlag Chemie GmbH, Weinheim, 1983.

Gruber, N.: Anthropogenic CO_2 in the Atlantic Ocean, Global Biogeochem. Cy., 12, 165–191, 1998.

Gruber, N., Sarmiento, J. L., and Stocker, T. F.: An improved method for detecting anthropogenic CO_2 in the oceans, Global Biogeochem. Cy., 10, 809–837, 1996.

Hauck, J., Hoppema, M., Bellerby, R. G. J., Völker, C., and Wolf-Gladrow, D.: Data-based estimation of anthropogenic carbon and acidification in the Weddell Sea on a decadal timescale, J. Geophys. Res., 115, C03004, doi:10.1029/2009JC005479, 2010.

Johnson, K. M., Sieburth, J. M., Williams, P. J., and Brändström, L.: Coulometric total carbon dioxide analysis for marine studies: automation and calibration, Mar. Chem., 21, 117–133, 1987.

Karstensen, J. and Quadfasel, D.: Water subducted into the Indian Ocean subtropical gyre, Deep Sea-Res. Pt. II, 49, 1441–1457, 2002.

Key, R. M., Tanhua, T., Olsen, A., Hoppema, M., Jutterström, S., Schirnick, C., van Heuven, S., Kozyr, A., Lin, X., Velo, A., Wallace, D. W. R., and Mintrop, L.: The CARINA data synthesis project: introduction and overview, Earth Syst. Sci. Data, 2, 105–121, doi:10.5194/essd-2-105-2010, 2010.

Lee, K., Millero, F. J., and Wanninkhof, R.: The carbon dioxide system in the Atlantic Ocean, J. Geophys. Res., 102, 15693–15707, 1997.

Lee, K., Choi, S.-D., Park, G.-H., Wanninkhof, R., Peng, T.-H., Key, R. M., Sabine, C. L., Feely, R. A., Bullister, J. L., Millero, A., and Kozyr, F. J.: An updated anthropogenic CO_2 inventory in the Atlantic Ocean, Global Biogeochem. Cy., 17, 1116, doi:10.1029/2003GB002067, 2003.

BGD
11, 6755–6792, 2014

Levine, N. M., Doney, S. C., Wanninkhof, R., Lindsay, K., and Fung, I. Y.: Impact of ocean carbon system variability on the detection of temporal increases in anthropogenic CO_2, J. Geophys. Res., 113, C03019, doi:10.1029/2007JC004153, 2008.

Levine, N. M., Doney, S. C., Lima, I., Wanninkhof, R., Bates, N. R., and Feely, R. A.: The impact of the North Atlantic Oscillation on the uptake and accumulation of anthropogenic CO_2 by North Atlantic Ocean mode waters, Global Biogeochem. Cy., 25, GB3022, doi:10.1029/2010GB003892, 2011.

Lewis, E. L. and Wallace, D. W. R.: Program Developed for CO_2 System Calculations, ORNL/CDIAC-105, Carbon Dioxide Information Analysis Center, Oak Ridge National Laboratory, US Department of Energy, Oak Ridge, 1998.

Lischka, S., Büdenbender, J., Boxhammer, T., and Riebesell, U.: Impact of ocean acidification and elevated temperatures on early juveniles of the polar shelled pteropod *Limacina helicina*: mortality, shell degradation, and shell growth, Biogeosciences, 8, 919–932, doi:10.5194/bg-8-919-2011, 2011.

McCartney, M. S.: Subantarctic mode water, in: A Voyage of Discovery, edited by: Angel, M., Pergamon, Elmsford, New York, 103–119, 1977.

McNeil, B. I. and Matear, R. J.: Southern Ocean acidification: a tipping point at 450-ppm atmospheric CO_2, P. Natl. Acad. Sci. USA, 105, 18860–18864, 2008.

McNeil, B. I., Tilbrook, B., and Matear, R.: Accumulation and uptake of anthropogenic CO_2 in the Southern Ocean, south of Australia between 1968 and 1996, J. Geophys. Res., 106, 31431–31445, 2001.

McNeil, B. I., Metzl, N., Key, R. M., Matear, R. J., and Corbiere, A.: An empirical estimate of the Southern Ocean air–sea CO_2 flux, Global Biogeochem. Cy., 21, GB3011, doi:10.1029/2007GB002991, 2007.

Mémery, L., Arhan, M., Alvarez-Salgado, X. A., Messias, M.-J., Mercier, H., Castro, C. G., and Ríos, A. F.: The water masses along the western boundary of the south and equatorial Atlantic, Prog. Oceanogr., 47, 69–98, 2000.

Metzl, N., Tilbrook, B., and Poisson, A.: The annual fCO_2 cycle and the air–sea CO_2 flux in the sub-Antarctic Ocean, Tellus B, 51, 849–861, 1999.

Mintrop, L., Perez, F. F., Gonzalez-Davila, M., Santana-Casiano, M. J., and Kortzinger, A.: Alkalinity determination by potentiometry: intercalibration using three different methods, Cienc. Mar., 26, 23–37, 2000.

BGD
11, 6755–6792, 2014

Murata, A., Kumamoto, Y., Sasaki, K. I., Watanabe, S., and Fukasawa, M.: Decadal increases of anthropogenic CO_2 in the subtropical South Atlantic Ocean along 30° S, J. Geophys. Res., 113, C06007, doi:10.1029/2007JC004424, 2008.

Orr, J. C., Fabry, V. J., Aumont, O., Bopp, L., Doney, S. C., Feely, R. A., Gnanadesikan, A., Gruber, N., Ishida, A., Joos, F., Key, R. M., Lindsay, K., Maier-Reimer, E., Matear, R., Monfray, P., Mouchet, A., Najjar, R. G., Plattner, G.-K., Rodgers, K. B., Sabine, C. L., Sarmiento, J. L., Schlitzer, R., Slater, R. D., Totterdell, I. J., Weirig, M.-F., Yamanaka, Y., and Yool, A.: Anthropogenic ocean acidification over the twenty-first century and its impact on calcifying organisms, Nature, 437, 681–686, 2005.

Orsi, A. H., Johnson, G. C., and Bullister, J. L.: Circulation, mixing, and production of Antarctic Bottom Water, Prog. Oceanogr., 43, 55–109, 1999.

Pai, S.-C., Gong, G., and Liu, K.-K.: Determination of dissolved oxygen in seawater by direct spectrophotometry of total iodine, Mar. Chem., 41, 343–351, 1993.

Peng, T.-H. and Wanninkhof, R.: Increase in anthropogenic CO_2 in the Atlantic Ocean in the last two decades, Deep-Sea Res. Pt. I, 57, 755–770, doi:10.1016/j.dsr.2010.03.008, 2010.

Peng, T.-H., Wanninkhof, R., and Feely, R. A.: Increase of anthropogenic CO_2 in the Pacific Ocean over the last two decades, Deep-Sea Res. Pt. II, 50, 3065–3082, 2003.

Pérez, F. F., Álvarez, M., and Ríos, A. F.: Improvements on the back-calculation technique for estimating anthropogenic CO_2, Deep-Sea Res. Pt. I, 49, 859–875, 2002.

Pérez, F. F., Vázquez-Rodríguez, M., Mercier, H., Velo, A., Lherminier, P., and Ríos, A. F.: Trends of anthropogenic CO_2 storage in North Atlantic water masses, Biogeosciences, 7, 1789–1807, doi:10.5194/bg-7-1789-2010, 2010.

Peterson, R. G. and Whitworth, T.: The subantarctic and polar fronts in relation to deep water masses through the Southwestern Atlantic, J. Geophys. Res., 94, 10817–10838, 1989.

Raven, J., Caldeira, K., Elderfield, H., Hoegh-Guldberg, O., Liss, P., Riebesell, U., Shepherd, J., Turley, C., and Watson, A.: Ocean Acidification Due to Increasing Atmospheric Carbon Dioxide, Policy Document 12/05, the Royal Society, London, 2005.

Revelle, R. and Suess, H.: Carbon dioxide exchange between atmosphere and ocean and the question of an increase of atmospheric CO_2 during the past decades, Tellus, 9, 18–27, 1957.

Ríos, A. F., Anderson, T. R., and Pérez, F. F.: The carbonic system distribution and fluxes in the NE Atlantic during Spring 1991, Prog. Oceanogr., 35, 295–314, 1995.

BGD
11, 6755–6792, 2014

Ríos, A. F., Pérez, F. F., Álvarez, M., Mintrop, L., González-Dávila, M., Santana Casiano, J. M., Lefèvre, N., and Watson, A. J.: Seasonal sea-surface carbon dioxide in the Azores area, Mar. Chem., 96, 35–51, 2005a.

Ríos, A. F., Johnson, K. M., Alvarez-Salgado, X. A., Arlen, L., Billant, A., Bingler, L. S., Branellec, P., Castro, C. G., Chipman, D. W., G. Roson and Wallace, D. W. R.: Carbon Dioxide, Hydrographic, and Chemical Data Obtained During the R/V *Maurice Ewing* Cruise in the South Atlantic Ocean (WOCE Section A17, 4 Janurary–21 March 1994), Carbon Dioxide Information Analysis Center, Oak Ridge National Laboratory, ORNL/CDIAC-148, NDP-084, 1–27, 2005b.

Ríos, A. F., Vázquez-Rodríguez, M., Padin, X. A., and Pérez, F. F.: Anthropogenic carbon dioxide in the South Atlantic western basin, J. Marine Syst., 83, 38–44, 2010.

Ríos, A. F., Velo, A., Pardo, P. C., M. Hoppema and Pérez, F. F.: An update of anthropogenic CO_2 storage rates in the western South Atlantic basin and the role of Antarctic Bottom Water, J. Marine Syst., 94, 197–203, doi:10.1016/j.jmarsys.2011.11.023, 2012.

Sabine, C. L. and Tanhua, T.:. Estimation of anthropogenic CO_2 inventories in the ocean, Ann. Rev. Mar. Sci., 2, 175–198, 2010.

Sabine, C. L., Key, R. M., Johnson, K. M., Millero, F. J., Poisson, A., Sarmiento, J. L., Wallace, D. W. R., and Winn, C. D.: Anthropogenic CO_2 inventory of the Indian Ocean, Global Biogeochem. Cy., 13, 179–198, 1999.

Sabine, C. L., Feely, R. A., Gruber, N., Key, R. M., Lee, K., Bullister, J. L., Wanninkhof, R., Wong, C. S., Wallace, D. W. R., Tilbrook, B., Millero, F. J., Peng, T.-H., Kozyr, A., Ono, R., and Ríos, A. F.: The oceanic sink for anthropogenic CO_2, Science, 305, 367–371, 2004.

Santana-Casiano, J. M., González-Dávila, M., Rueda, M.-J., Llinás, O., and González-Dávila, E.-F.: The interannual variability of oceanic CO_2 parameters in the northeast Atlantic subtropical gyre at the ESTOC site, Global Biogeochem. Cy., 21, GB1015, doi:10.1029/2006GB002788, 2007.

Sarmiento, J. L., Gruber, N., Brzezinski, M. A., and Dunne, J. P.: High-latitude controls of thermocline nutrients and low latitude, Nature, 427, 56–60, 2004.

Takahashi, T., Sutherland, S. C., Wanninkhof, R., C. Sweeney, Feely, R. A., Chipman, D. W., Hales, B., Friederich, G., Chavez, F., Sabine, C., Watson, A., Bakker, D. C. E., Schuster, U., Metzl, N., Yoshikawa-Inoue, H., Ishii, M., Midorikawa, T., Nojiri, Y., Kortzinger, A., Steinhoff, T., Hoppema, M., Olafsson, J., Arnarson, T. S., Tilbrook, B., Johannessen, T., Olsen, A., Bellerby, R., Wong, C. S., Delille, B., Bates, N. R., and de Baar, H. J. W.: Climatological

BGD
11, 6755–6792, 2014

mean and decadal change in surface ocean pCO_2, and net sea–air CO_2 flux over the global oceans, Deep-Sea Res. Pt. II, 56, 554–577, doi:10.1016/j.dsr2.2008.12.009, 2009.
Talley, L. D.: Antarctic intermediate water in the South Atlantic, in: The South Atlantic: Present and Past Circulation, edited by: Wefer, G., Berger, H. H., Siedler, G., and Webb, D., Springer, 1996.
Touratier, F., Azouzi, L., and Goyet, C.: CFC-11, $\delta^{14}C$ and ^3H tracers as a means to assess anthropogenic CO_2 concentrations in the ocean, Tellus B, 59, 318–325, 2007.
van Heuven, S. M. A. C., Pierrot, D., Lewis, E., and Wallace, D. W. R.: MATLAB Program Developed for CO_2 System Calculations, ORNL/CDIAC-105b, Carbon Dioxide Information Analysis Center, Oak Ridge National Laboratory, US Department of Energy, Oak Ridge, Tennessee, doi:10.3334/CDIAC/otg.CO2SYS MATLAB v1.1, 2011a.
van Heuven, S. M. A. C., Hoppema, M., Huhn, O., Slagter, H. A., and de Baar, H. J. W.: Direct observation of increasing CO_2 in the Weddell Gyre along the Prime Meridian during 1973–2008, Deep-Sea Res. Pt. II, 58, 2613–2635, doi:10.1016/j.dsr2.2011.08.007, 2011b.
Vázquez-Rodríguez, M., Touratier, F., Lo Monaco, C., Waugh, D. W., Padin, X. A., Bellerby, R. G. J., Goyet, C., Metzl, N., Ríos, A. F., and Pérez, F. F.: Anthropogenic carbon distributions in the Atlantic Ocean: data-based estimates from the Arctic to the Antarctic, Biogeosciences, 6, 439–451, doi:10.5194/bg-6-439-2009, 2009a.
Vázquez-Rodríguez, M., Padin, X. A., Ríos, A. F., Bellerby, R. G. J., and Pérez, F. F.: An upgraded carbon-based method to estimate the anthropogenic fraction of dissolved CO_2 in the Atlantic Ocean, Biogeosciences Discuss., 6, 4527–4571, doi:10.5194/bgd-6-4527-2009, 2009b.
Vázquez-Rodríguez, M., Pérez, F. F., Velo, A., Ríos, A. F., and Mercier, H.: Observed acidification trends in North Atlantic water masses, Biogeosciences, 9, 5217–5230, doi:10.5194/bg-9-5217-2012, 2012.
Wallace, D. W. R.: Monitoring Global Ocean Carbon Inventories, OOSDP Background Report No. 5, Texas A&M University, College Station, Texas, USA, 1995.
Wanninkhof, R., Doney, S. C., Bullister, J. L., Levine, N. M., Warner, M., and Gruber, N.: Detecting anthropogenic CO_2 changes in the interior Atlantic Ocean between 1989 and 2005, J. Geophys. Res., 115, C11028, doi:10.1029/2010JC006251, 2010.
Waugh, D. W., Hall, T. M., McNeil, B. I., Key, R., and Matear, R. J.: Anthropogenic CO_2 in the oceans estimated using transit time distributions, Tellus B, 58, 376–389, doi:10.1111/j.1600-0889.2006.00222.x, 2006.

BGD
11, 6755–6792, 2014

Winkler, L. W.: Die Bestimmung des im Wasser gelösten Sauerstoffes, Chem. Ber., 27, 2843–2855, 1888.

Wong, A. P. S., Bindoff, N. L., and Church, J. A.: Large-scale freshening of intermediate waters in the Pacific and Indian oceans, Nature, 400, 440–443, 1999.

Yool, A., Oschlies, A., Nurser, A. J. G., and Gruber, N.: A model-based assessment of the TrOCA approach for estimating anthropogenic carbon in the ocean, Biogeosciences, 7, 723–751, doi:10.5194/bg-7-723-2010, 2010.

BGD

11, 6755–6792, 2014

Table 1. Difference between the calculated coefficients of the applied eMLR for various density intervals.

Min density	Max density	Mean Layer Depth (m)	*a*	$Si(OH)_4$	NO_3	Sal	Theta	AOU	Pressure	rmse	R^2	*n*
Sigma-θ												
20.0	23.5	31	132	5.67	−130.26	−12.47	10.73	−0.12	0.16	7.61	0.98	40
23.5	24.5	50	−190	−6.97	15.19	2.30	3.63	0.15	0.04	6.26	0.95	30
24.5	25.0	53	899	23.25	−12.86	−31.74	8.84	0.23	0.37	4.98	0.99	12
25.0	25.4	57	549	3.32	−0.64	−18.85	4.47	−0.21	0.31	5.54	0.99	18
25.4	26.2	107	−603	6.54	0.36	17.33	−2.68	−0.21	0.05	3.78	0.99	31
26.2	26.4	160	−109	0.97	1.57	1.68	1.42	−0.15	0.03	2.11	1.00	21
26.4	26.6	196	139	0.93	−0.13	−4.83	0.68	0.05	0.01	2.35	1.00	33
26.6	26.8	259	77	1.31	1.51	−4.29	3.40	−0.17	0.01	1.65	1.00	30
26.8	27.0	310	288	1.33	1.70	−10.90	5.14	−0.19	0.01	1.64	1.0	42
27.0	27.2	431	82	−0.12	−0.97	−1.59	−2.97	0.16	0.00	1.14	1.0	50
27.2	27.4	672	730	0.21	−1.29	−20.88	0.74	0.16	0.00	2.07	0.99	37
27.4	27.5	991	−1466	−0.01	1.77	42.62	−0.63	−0.35	−0.01	1.37	0.98	22
Sigma-2												
27.5	36.7	1108	−141	−0.24	3.84	2.11	5.01	−0.52	0.01	1.50	0.99	40
36.7	36.8	1279	−199	−0.35	4.05	4.88	−0.92	−0.50	0.00	0.98	1.00	21
36.8	36.9	1531	−3210	−0.67	4.15	92.33	−17.46	−0.15	−0.01	1.25	1.00	20
36.9	36.9	1614	−1563	−0.29	3.42	44.16	−6.22	−0.25	0.00	1.15	1.00	16
36.9	37.0	1946	−3314	−0.75	6.28	93.81	−14.05	−0.33	0.00	2.27	1.00	48
37.0	37.1	2586	−3038	−0.54	4.80	85.85	−9.70	−0.20	0.00	0.74	1.00	95
Sigma-4												
37.1	45.9	3050	−474	0.18	1.33	11.41	13.33	−0.12	0.01	0.73	0.99	29
45.9	46.0	3730	−51	0.35	2.02	0.07	13.57	−0.54	0.00	1.18	1.00	61
46.0	46.0	4195	22 023	−0.34	−1.72	−628.87	20.07	−0.80	0.00	1.43	1.00	18
46.0	46.1	4582	7689	−0.33	0.93	−219.90	9.91	−0.38	0.00	1.04	0.99	28
46.1	60.0	5108	−47 999	0.63	1.291	1385.48	−55.32	−1.04	−0.01	1.09	0.89	25

BGD
11, 6755–6792, 2014

Table 2. The calculated rates of increase of C_{ant} and rates of decrease of pH along the section, listed per water mass. The identification criteria for each water mass are provided. Error represents $2\sigma/N^{0.5}$.

Water Mass	Density Range	Latitude	Pressure (dbar)	dC_{ant}/dt ($\mu mol\,kg^{-1}\,yr^{-1}$)	dC_{ant}/dt[a] ($\mu mol\,kg^{-1}\,yr^{-1}$)	dpH/dt (yr^{-1})
SACW	$\sigma^{\theta}20$–$\sigma^{\theta}26.8$	23–18° S	90–160	0.99 ± 0.14	0.90 ± 0.04	−0.0016
SAMW	$\sigma^{\theta}26.8$–$\sigma^{\theta}27.1$	50–48° S	90–160	0.53 ± 0.11	0.53 ± 0.02	−0.0014
AAIW	$\sigma^{\theta}27.1$–$\sigma^{\theta}27.4$	50–48° S	360–450	0.36 ± 0.06	0.36 ± 0.06	−0.0010
*u*CDW	$\sigma^{\theta}27.4$–$\sigma^{3}41.47$	50–49° S	1400–1800	0.33 ± 0.07	0.16 ± 0.04	−0.0010
*u*NADW	$\sigma^{\theta}27.4$–$\sigma^{3}41.47$	10–15° N	1600–1800	0.20 ± 0.03	0.16 ± 0.04	−0.0005
/CDW	$\sigma^{3}41.47$–$\sigma^{4}45.9$	50–48° S	3250–3750	0 ± 0.06	0.08 ± 0.04	0.0000
/NADW	$\sigma^{3}41.47$–$\sigma^{4}45.9$	10–15° N	3000–3500	0 ± 0.02	0.08 ± 0.04	0.0000

[a] Values from Ríos et al. (2012).

BGD
11, 6755–6792, 2014

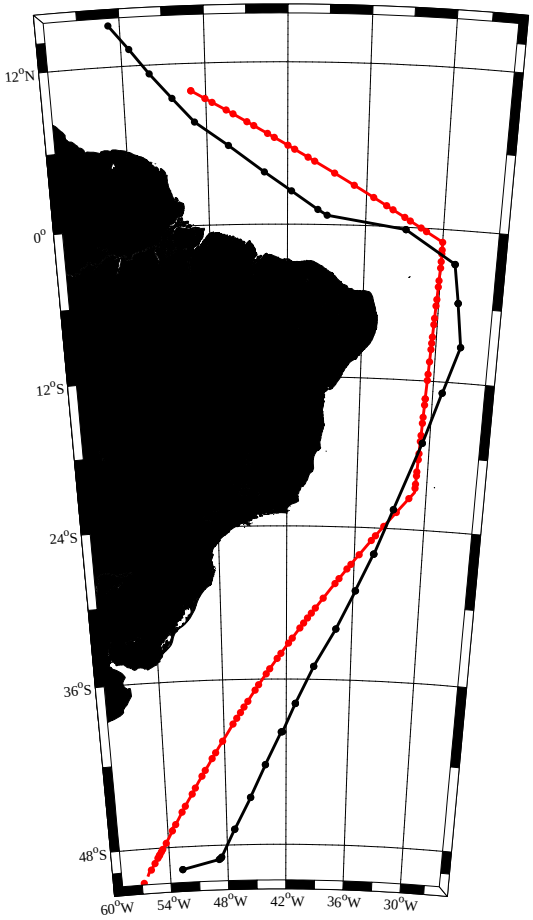

Fig. 1. Cruise tracks from both cruises with used stations (black represents the WOCE '94 A17 line, red represents the GEOTRACES-NL (2010/2011) expeditions).

BGD
11, 6755–6792, 2014

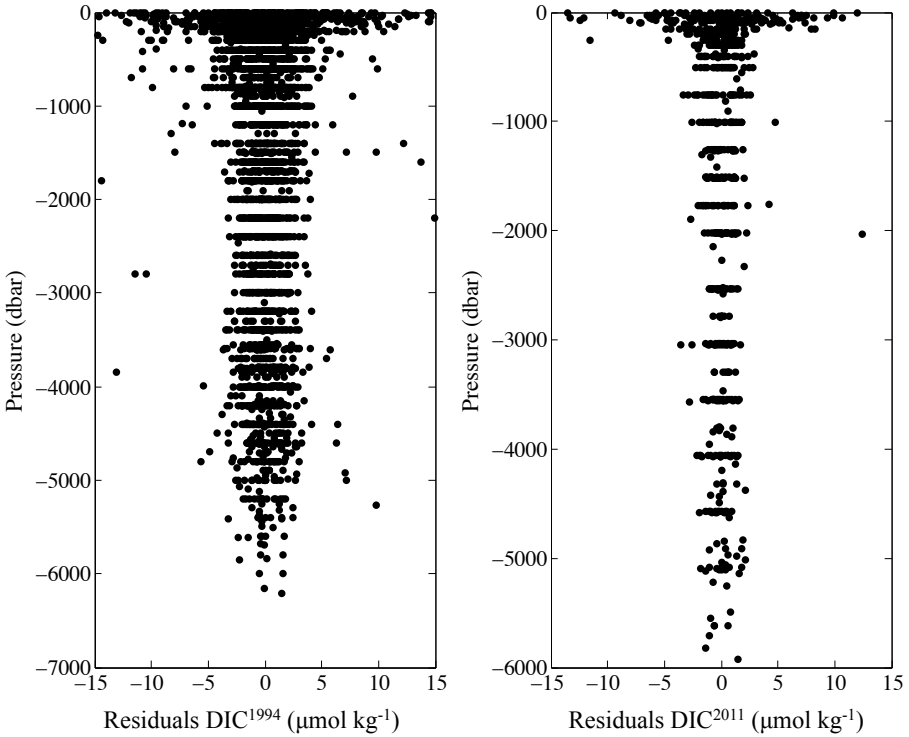

Fig. 2. The residuals of the MLR fits of the **(a)** WOCE '94 A17 and **(b)** GEOTRACES-NL (2010/2011) datasets.

BGD
11, 6755–6792, 2014

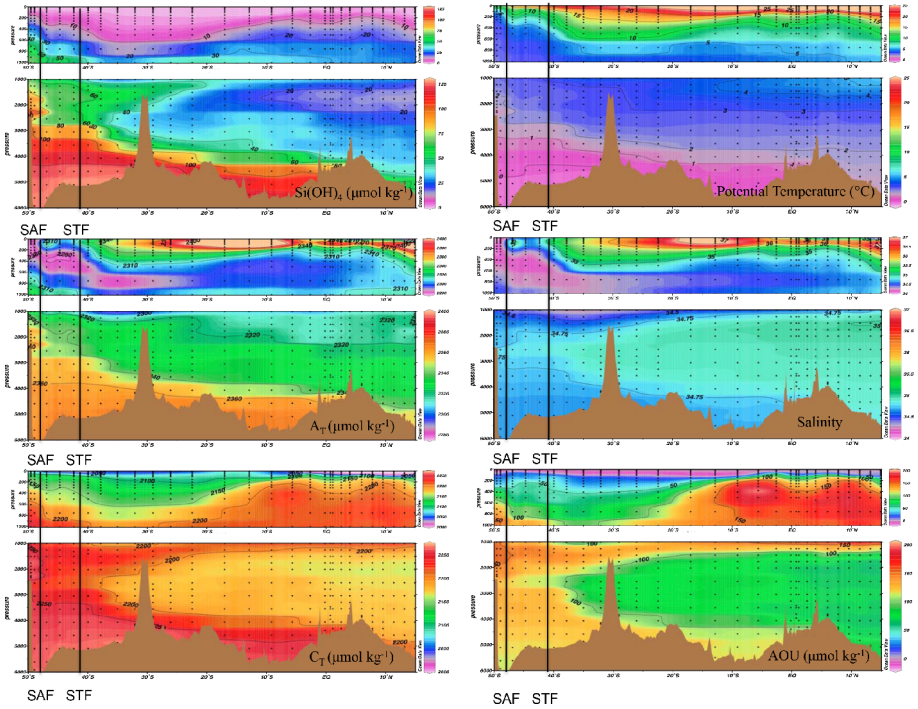

Fig. 3. Section distributions of temperature (°C), salinity, AOU (μmol kg^{-1}), silicate (μmol kg^{-1}), A_T (μmol kg^{-1}) and DIC (μmol kg^{-1}). Black solid lines represent the SubAntarctic front (SAF) and Subtropical Front (STF) at the surface.

BGD
11, 6755–6792, 2014

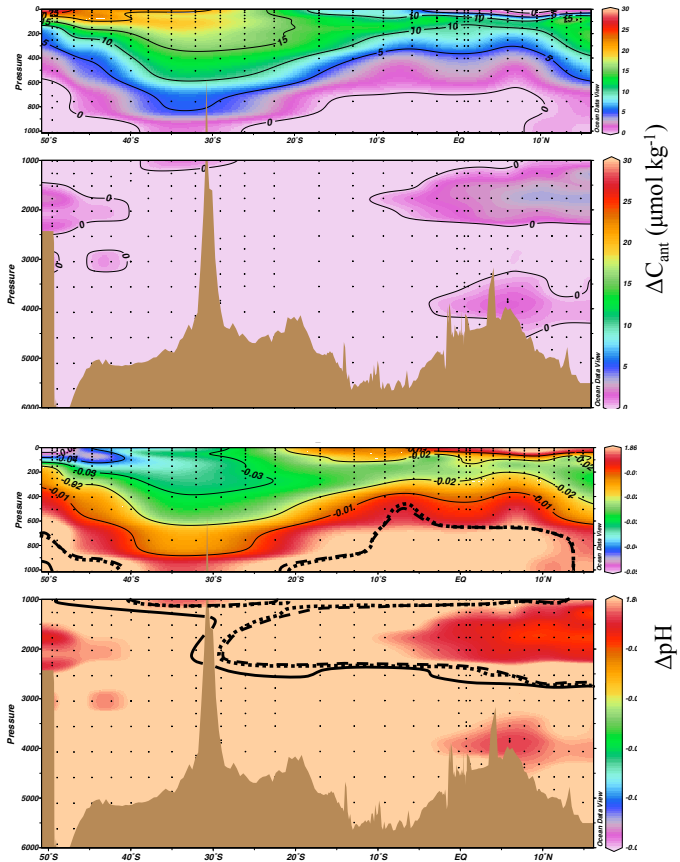

Fig. 4. (a) Distribution of $\Delta C_{ant}^{1994–2011}$ ($\mu mol\,kg^{-1}$), calculated using the eMLR approach. **(b)** Distribution of the $\Delta pH^{1994–2011}$ associated with $\Delta C_{ant}^{1994–2011}$. The aragonite saturation horizon (Ω_{Ar}) is marked on for pre-industrial times (solid line), 1994 (dashed line) and 2011 (dotted line).

BGD
11, 6755–6792, 2014

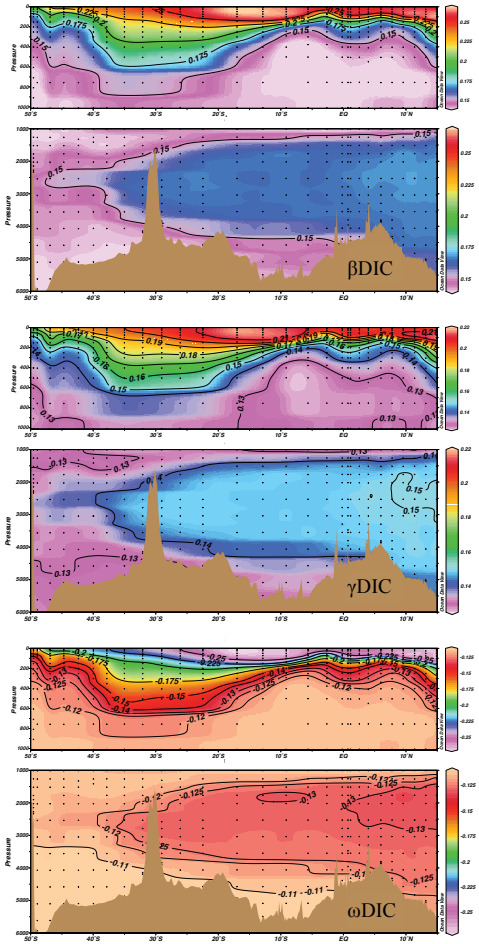

Fig. 5. Distribution of the three buffering factors relating to DIC; βDIC, γDIC, and ωDIC (mmol kg^{-1}).

BGD
11, 6755–6792, 2014

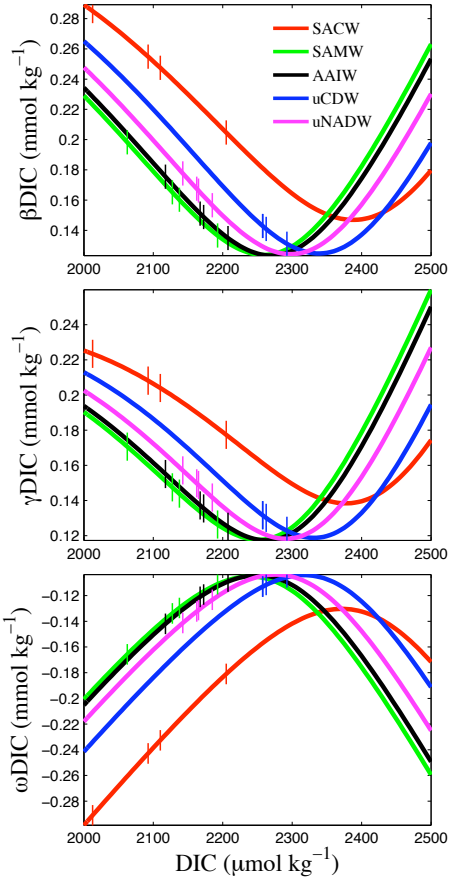

Fig. 6. The buffer factors of each water mass over a range of DIC concentrations. The vertical lines denote the DIC concentration in pre-industrial times, 1994, 2011 and the projected concentration in 2110.

BGD
11, 6755–6792, 2014